Proc. Natl. Acad. Sci. USA
Vol. 77, No. 6, pp. 3105–3109, June 1980
Chemistry

Role of the chlorophyll dimer in bacterial photosynthesis

(electron transfer/charge separation/light energy storage)

ARIEH WARSHEL

Department of Chemistry, University of Southern California, Los Angeles, California 90007

Communicated by Martin D. Kamen, March 18, 1980

ABSTRACT **The role of a special dimer (D) of bacteriochlorophyll molecules in bacterial photosynthesis was examined by calculations of the rates of electron transfer reactions in a system of the dimer and a bacteriopheophytin (BPh) molecule. It was found that the dependence of the potential surfaces of D on the distance between the monomers allows a fast light-induced electron transfer from D to BPh but only a slow back reaction (reduction of D^+ by BPh^-). The same potential surfaces allow efficient reduction of D^+ by cytochrome *c*. Possible advantages of greatly different values of the electronic matrix elements for the forward and back reactions are pointed out. It is suggested that the electrostatic interaction between D^+ and an ionized group of the protein might play an important role in the photosynthetic reaction.**

The first step in bacterial photosynthesis involves absorption of light by a special dimer (D) of bacteriochlorophyll (BChl) molecules and transfer of an electron from the excited dimer (D^*) to a primary acceptor (I), probably a bacteriopheophytin (BPh) molecule, to form the system D^+I^-. The electron is then transferred to a secondary acceptor, Q, and D^+ is reduced by cytochrome *c* (C) (for recent views see refs. 1 and 2). The measured rates of the various competing processes involved in these reactions (2) provide a kinetic description of an extremely efficient system (see Fig. 1). The excited dimer ejects an electron before its deactivation by radiative and radiationless processes, while the back reaction, $D^+I^- \rightarrow DI$, is blocked so that it does not compete with electron transfer from I^- to Q. This kinetic information does not reveal the molecular basis of the photosynthetic reaction and does not explain why nature chose a dimer as the primary acceptor.

This work examines the role of the special dimer by model calculations of the rate of light-induced electron transfer from the BChl dimer to a BPh molecule. The calculations indicate that the weak noncovalent bond between the two BChl monomers provides an efficient "trap" for the excitation energy and may account for the rate difference between the forward and back reactions. The possible role of the electrostatic interaction between the dimer and an ionized group of the protein is also considered. It is pointed out that such interaction may slow the back reaction by polarizing D^+ and shifting the center of positive charge further from I^-.

Theoretical treatment of electron transfer reactions

The theory of electron transfer processes (3–6) is illustrated in Fig. 2. The figure describes the potential surfaces of the combined donor, A, and acceptor, B, system. In the quadratic approximation the potential surfaces of the reactants AB (V_1) and the products A^+B^- (V_2) can be represented by:

$$V_1 = \frac{1}{2} hc(\bar{\nu}_1 Q_1^2 + \bar{\nu}_2 Q_2^2) \qquad [1]$$

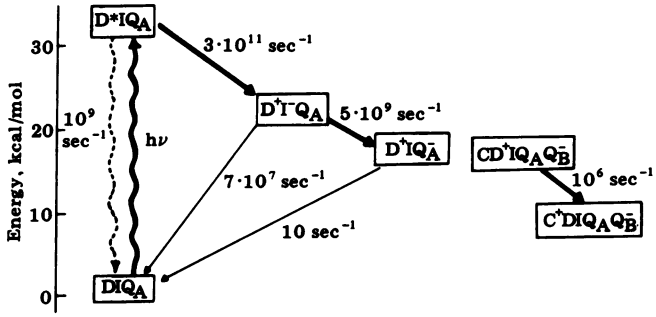

FIG. 1. Rates of electron transfer along different possible reaction pathways in the reaction center of the photosynthetic bacteria. D, I, Q, and C are, respectively, the special dimer, the primary acceptor, the secondary acceptor, and cytochrome *c*. The relative energies of the various states are indicated.

$$V_2 = \frac{1}{2} hc(\bar{\nu}_1(Q_1 - \Delta_1)^2 + \bar{\nu}_2(Q_2 - \Delta_2)^2),$$

where $\bar{\nu}$ and Δ are, respectively, the average vibration frequencies (in cm^{-1}) and origin shifts of the dimensionless normal coordinates Q[$Q = (4\pi^2\nu/h)^{1/2}q$, where q is the mass-scaled Cartesian normal mode]. In the high temperature limit, when the thermal energy is larger than $hc\bar{\nu}_1$ and $hc\bar{\nu}_2$, the electron transfer rate is given by a two-dimensional representation of Hopfield's expression (4)

$$k = (2\pi\sigma_{AB}^2/\hbar)(4\pi(\alpha_1 + \alpha_2)k_bT)^{-1/2} \exp\{-E^\ddagger/k_bT\} \qquad [2]$$

where σ_{AB} is the matrix element of the Hamiltonian between the electronic wave functions of A and B, k_b is the Boltzmann constant, $\alpha_i = hc\bar{\nu}_iS_i$, and $S_i = \frac{1}{2}\Delta_i^2$. Fig. 2 demonstrates that the activation energy, which satisfies the relation $E^\ddagger = (\Delta E_0 - \alpha_1 - \alpha_2)^2/4(\alpha_1 + \alpha_2)$, is simply the energy needed to reach the intersection of V_1 and V_2, the locus of points where an electron transfer process that conserves energy involves no change in nuclear coordinates. In the high temperature case it is possible to treat the electron transfer problem by the semiclassical trajectory approach of ref. 8. For small σ_{AB}, when the diabatic approximation is valid this gives essentially the Landau–Zener transition probability (8) which, when substituted into the rate expression in transition rate theory, gives exactly the same expression as Eq. 2.

In the low temperature region electron transfer can be considered tunneling from the 0 vibronic level of AB to the vibronic levels of A^+B^- that satisfy the requirement of conservation of energy. The rate of such a process is given by standard first-order perturbation theory as:

$$k = 2\pi(\sigma_{AB}^2/\hbar) \sum_n C(0,n)^2\, \delta(\Delta E_0 - E_n), \qquad [3]$$

The publication costs of this article were defrayed in part by page charge payment. This article must therefore be hereby marked "*advertisement*" in accordance with 18 U. S. C. §1734 solely to indicate this fact.

Abbreviations: BChl, bacteriochlorophyll; BPh, bacteriopheophytin; D, dimer of BCl; I, primary acceptor; Q, secondary acceptor; C, cytochrome *c*; QCFF/PI, quantum mechanical extension of the consistent force field method to π electron molecules.

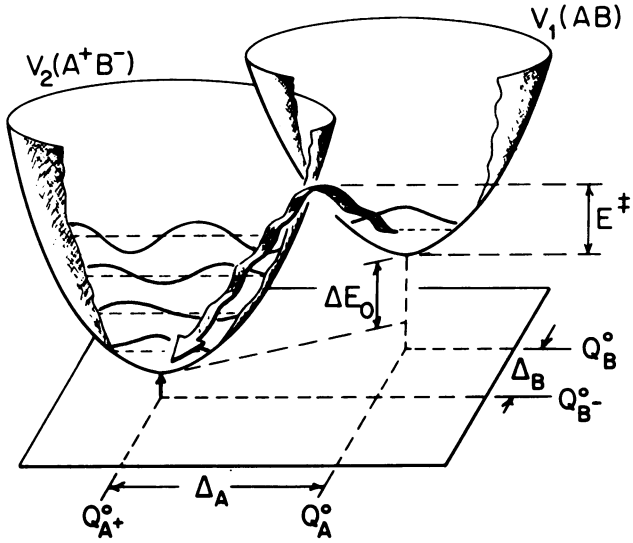

FIG. 2. Schematic description of electron transfer between donor, A, and acceptor, B. V_1 and V_2 are the potential surface, for the AB and A^+B^- systems, respectively. These potential surfaces are drawn along two representative coordinates Q_A and Q_B. The Q^o are the equilibrium coordinates; Δ and $E^\ddagger$ are, respectively, the indicated origin shift and the activation energy for thermally induced electron transfer. The figure also shows some vibrational energy levels which provide channels for quantum mechanical tunneling.

where $C(\mathbf{0},\mathbf{n})$ is the Franck–Condon overlap integral, $\mathbf{n}$ is the vector (n_1,n_2) of the vibronic quantum numbers of A^+B^-, and $E_n = \Sigma_i\, hc\bar{\nu}_i(n_i + \frac{1}{2})$. Using the analytical expression for $C(\mathbf{0},\mathbf{n})$ (7, 9) gives

$$k = 2\pi(\sigma^2_{AB}/\hbar)(hc\bar{\nu}_1)^{-1}\exp\{-(S_1 + S_2)\}$$
$$\sum_{n_2} S_1^{n_1[n_2]}\, S^{n_2}/(n_1[n_2]!n_2!), \quad [4]$$

where $n_1[n_2] = (\Delta E_0 - n_2hc\bar{\nu}_2)/hc\bar{\nu}_1$.

In the intermediate temperature case when $k_BT \gg hc\bar{\nu}_1$ and $k_BT \ll hc\bar{\nu}_2$, $\bar{\nu}_1$ can be treated classically and $\bar{\nu}_2$ quantum mechanically. In this case the rate is given by (5):

$$k = (2\pi\sigma^2_{AB}/\hbar)(4\pi\alpha_1k_bT)^{-1/2}$$
$$\sum_{n_2} \exp\{-S_2 - E_1^\ddagger(n_2)/k_bT)\}S_2^{n_2}/n_2! \quad [5]$$

where

$$E_1^\ddagger(n_2) = [(\Delta E_0 - n_2hc\bar{\nu} - \alpha_1)^2/(4\alpha_1). \quad [6]$$

If the potential along Q_1 is not harmonic (as is the case here), $E^\ddagger(n_2)$ is approximated by the intersection of $(V_2 + n_2hc\bar{\nu})$ with V_1.

Previous studies of electron transfer in biological systems considered the one-dimensional version of Eqs. 2 and 4 and tried to extract parameters S and $\bar{\nu}$ from the experimental dependence of the rate on temperature (2, 4, 5). The parameters obtained by this phenomenological approach have not been related to the detail structure of the reaction center.

Here I take a quite different approach, calculating V_1 and V_2 for assumed relative geometries of I and D and examining whether they reproduce the experimental rates.

Potential surface of the BChl dimer

The potential surface of different geometries of the BChl dimer was evaluated by the quantum mechanical extension of the consistent force field method to π electron molecules (QCFF/PI method) (10) as described in ref. 11. In the absence of direct structural information, I introduce the working hypothesis that the overlap interaction between the monomers is significant in the real dimer system. Therefore, I limit the studies to geometries with significant overlap. This assumption is supported by a recent analysis of the red shift in aggregated chlorophylls (11) and to some extent by the spin distribution of D^+, which indicates equal sharing of the odd electron by the two BChl molecules (12). This paper presents the calculated potential surface for the geometry shown in Fig. 3, which was the relative crystal geometry of polymeric Chl-a (11). Other parallel orientations, including the C_2 configuration proposed by Katz *et al.* (1), gave essentially the same type of potential surface.[a]

The potential surface of the dimer system of Fig. 3 is presented in Fig. 4. As seen from the figure, the repulsion between the monomers upon decrease of the interplanar distance z is much stronger in the ground state, D, than in D^+. This result, which is common to most dimers, can be understood qualitatively from the orbital diagram in Fig. 4, which shows the dimer molecular orbitals split by the overlap interaction between the monomers. In the dimer ground state the π_a-π_b antibonding molecular orbital is occupied by two electrons, whereas in D^* and D^+ it is occupied by only one electron. Therefore, the bonding interaction between the monomers is significantly stronger in D^+ and D^* than in D. The result of the balance between the bonding interaction (linearly proportional to the

[a] The configuration presented in Fig. 3 is in no way a prediction of the configuration of the special dimer. However, the qualitative features of the potential surface are probably relevant to any dimer with significant overlap.

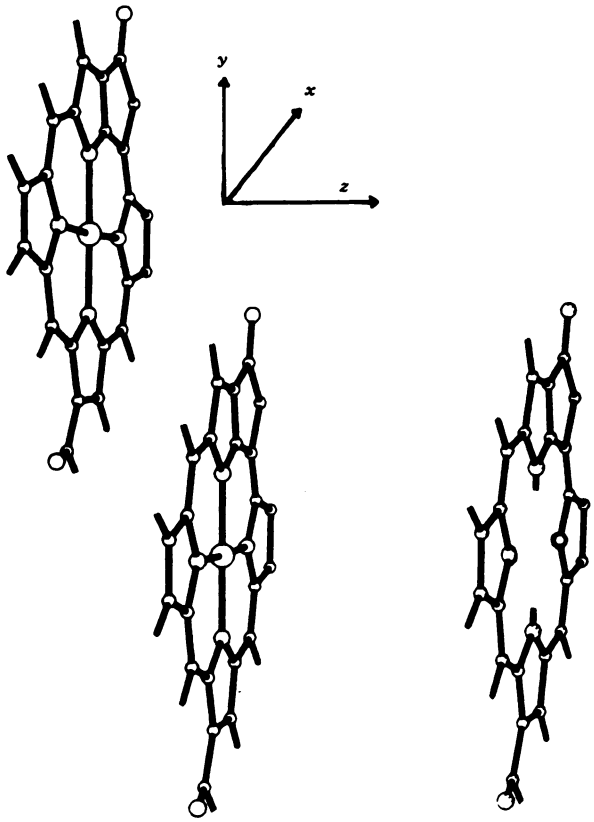

FIG. 3. The system studied in the present work. A BChl dimer in the stacking orientation of crystalline polymeric chlorophyll and a BPh molecule 5 Å from the nearest BChl; z is the distance between the planes of the BChl monomers.

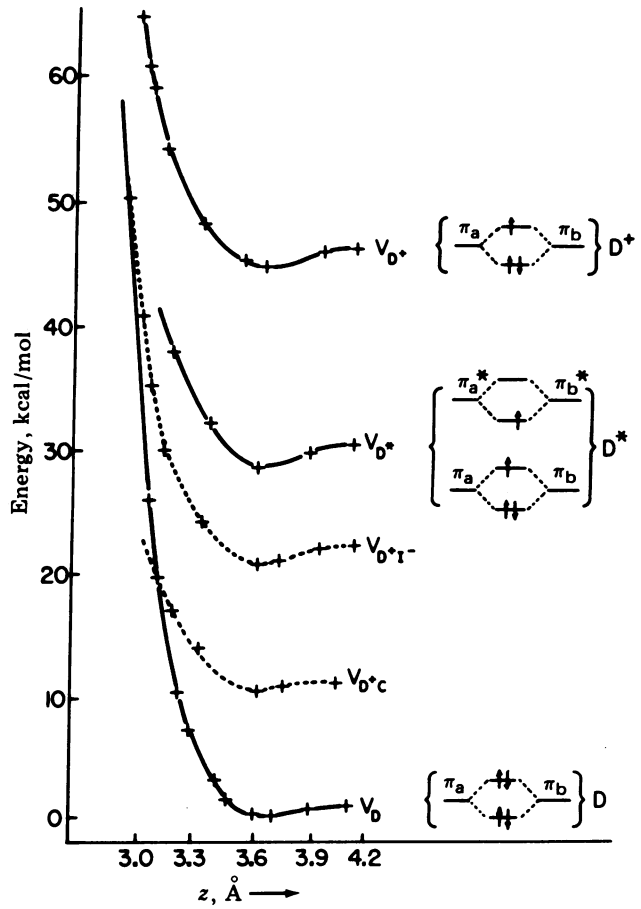

FIG. 4. Calculated potential surface of D, D*, and D^+ as function of the intermonomer distance, z. No significant origin shift was found along the x and y intermonomer coordinates. The figure also presents the potential surface for the D^+I^- system. This surface is obtained by shifting the D^+ surface to a point where its minimum is 20.7 kcal above the ground state minimum to reproduce the experimental estimate. Similarly, the potential surface for D^+C is obtained by shifting the minimum of the D^+ surface to 10 kcal/mol above the ground state minimum to reproduce the experiment estimate of the energy difference between D^+C and DC. a and b in the molecular orbital diagrams indicate the two monomers.

overlap) and the repulsive interaction (quadratically proportional to the overlap) gives much steeper potential to D than to D* and D^+ as a function of z.

In order to evaluate the potential surface for the electron transfer reaction between D and a BPh molecule, I consider, in addition to the soft z coordinate, other coordinates that might change their equilibrium values as a result of an electronic transition. This was done by calculating the potential surface of BPh and BPh^- by using the QCFF/PI potentials (10) and evaluating the origin shifts, S_i, and vibrational frequencies, $\bar{\nu}_i$, by the approach of refs. 9 and 10. It was found that only the 110, 320, 700, 1210, 1360, and 1400 cm^{-1} normal modes have significant S values (0.4, 0.25, 0.12, 0.08, 0.18, and 0.12 respectively). The S values for intramonomer vibrations in D were found to be significant for the modes at 100, 224, 750, 1200, 1400, and 1520 cm^{-1}. The corresponding S values are 0.06, 0.03, 0.02, 0.03, 0.02, and 0.04 for D → D* and 0.30, 0.10, 0.07, 0.01, 0.09, and 0.10 for D* → D^+. In order to simplify the discussion in this paper I combine the effect of the four high-frequency stretching modes in one effective mode $\bar{\nu}_r$ with stretching frequency of 1400 cm^{-1} and an effective S value of 0.7 (these effective values given the best fit to electron transfer calculations that used all the high-frequency modes). The origin shifts of the two low-frequency modes were neglected because they are much smaller than the S value of the low-frequency z mode (including these S values in electron transfer calculation give essentially the same results as those presented below).

Electron transfer on DI potential surfaces

By using the calculated potential surface of the dimer and the BPh monomer I constructed qualitative potential surfaces for the donor–acceptor (DI) system (Fig. 5). These surfaces are constructed from the sum of the D and I potential surfaces where the height of the minimum of the D^+I^- system relative to the minimum of the DI system is determined from experimentally estimated redox potentials (2) and the height of the D*I surface is determined by the DI → D*I excitation energy. Additional details are given in the legend to Fig. 5.

A qualitative examination of the potential surfaces of Fig. 5 demonstrates that the D*I → D^+I^- process is very fast because it does not involve any significant activation energy, whereas the reaction channel of surface crossing along the z direction in the D^+I^- → DI process requires such a high activation energy (30 kcal/mol) that it is essentially blocked and can occur only by radiationless transitions to the high-frequency combined mode ν_r of D.

In order to examine these features in a more quantitative way it is necessary to calculate the various rates of electron transfer. Such calculations are summarized in Table 1. The calculations use z and r as effective coordinates. The rates are calculated from Eq. 5, which is rewritten as:

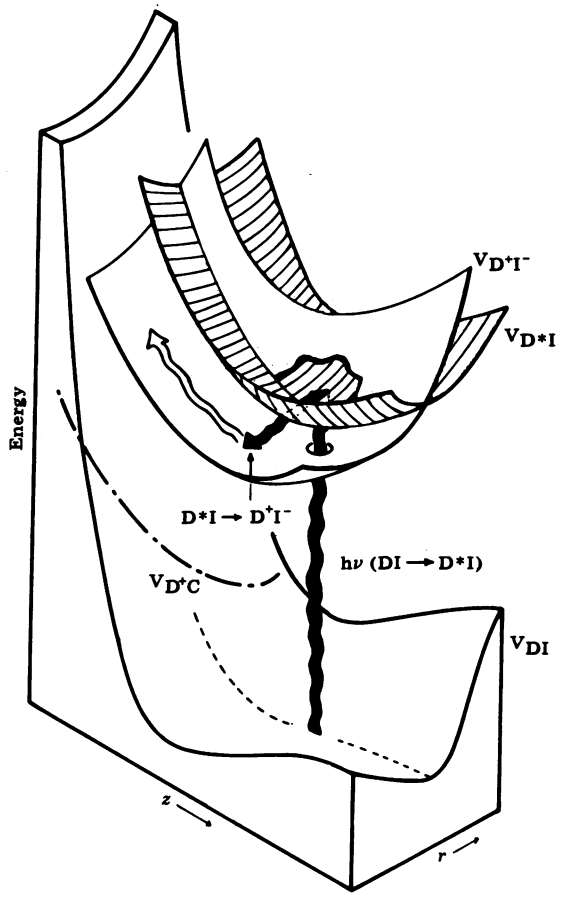

FIG. 5. Potential surfaces for the DI, D*I, D^+I^-, and D^+C surfaces. The surfaces are given as functions of the z coordinate and the effective stretching normal mode (see text). The heights of the minima of the surfaces are determined from experimental estimates. Note that the D^+C potential surface may be at lower energy (see *Discussion*).

Table 1. Calculations of electron transfer rates in the DI and DC systems[a]

Process	$E_z^{\ddagger}(n_r)$	n_r	$\Delta E_0 - n_r hc\bar{\nu}$	$S_z^*(S_z)$	S_r	σ[b]	k_{calc}[c]	k_{obs}	T
$D^*I \rightarrow D^+I^-$	4.2	0	6.0	4.5 (1)	0.7	0.20	1×10^9	—	300
	0.1	1	2.0	2.0	0.7	0.20	3×10^{11}	3×10^{11}	300
$D^+I^- \rightarrow DI$	30.0	0	20.7	9.4 (2)	0.7	0.07	10^{-13}	—	300
	3.1	4	4.7	1.5	0.7	0.07	2×10^7	10^8	300
$D^+C \rightarrow DC^+$	10.0	0	10.0	5.9 (2)	0.7	0.002	10^{-1}	—	300
	1.5	2	2.0	1.3	0.7	0.002	10^6	10^6	300
	1.5	2	2.0	1.3	0.7	0.002	10^4	3×10^2	100
	1.5	2	2.0	1.3	0.7	0.002	10^4	3×10^2	0

[a] $E_z^{\ddagger}(n_r)$ is the activation energy for the surface crossing process (for the given n_r) that involves motion along the z coordinate. This value is obtained from the actual intersection of V_2 and $V_1 + n_r hc\bar{\nu}_r$ rather than from the quadratic approximation of Eq. 6. S_z^* is the effective S_z value that gives $E_z^{\ddagger}(n)$ by using Eq. 6 with a value of $\bar{\nu}_z = 100\ cm^{-1}$, which is obtained by fitting quadratic potential to the ground state surface. The calculated value of S_z is given in parentheses and is not relevant to the calculated rates because the potential surfaces are of very different curvature. The average vibrational frequency $\bar{\nu}_r$ of the effective stretching mode is $1400\ cm^{-1}$. The units of $E^{\ddagger}$, ΔE_0, and σ are kcal/mol. k_{calc} and k_{obs} are the calculated and observed rates in sec^{-1}. T is the absolute temperature.

[b] The σ values for the DI system were calculated for the orientation in Fig. 3 holding I 5 Å from the nearest monomer of D. σ is evaluated by averaging the σ values for displacements of ±1 Å in the x direction (see text). σ for the DC system is evaluated by fitting the calculated and observed rates at 300 K.

[c] k_{calc} for the low temperature range is evaluated by using the rigorous quantum mechanical overlap integrals of ref. 7 rather than by Eq. 4, which is not accurate in our case when $\bar{\nu}_z$ of V_1 is significantly different from $\bar{\nu}_z$ of V_2.

$$k = \sum_i k_z(n_r)k_r(n_r) = k_z(0) + k_z(1)k_r(1) + \cdots k_z(4)k_r(4), \quad [7]$$

where

$$k_z(n_r) = 2\pi(\sigma^2/\hbar)(4\pi\alpha_z k_b T)^{-1/2} \exp\{-E_z^{\ddagger}(n_r)/k_b T\} \quad [8]$$

and

$$k_r(n_r) = \exp\{-S_r\}\, S_r^{n_r}/n_r! \quad [9]$$

The matrix elements σ are evaluated by placing I in an orientation parallel to its nearest BChl neighbor in D (Fig. 3) at a distance of 5 Å, which reproduces the observed rate for the $D^*I \rightarrow D^+I^-$ process. This, of course, does not represent any attempt to locate the relative position of I, but it allows for preliminary estimates of the change in σ between the forward and backward reactions. In the parallel orientation, σ for the forward reaction involves two π orbitals with large overlap in the parallel orientation whereas the σ for the back reaction involves the orthogonal π and π^* orbitals with small overlap in the parallel orientation.[b] With D and I fixed, we obtain a ratio of 100 between the σ of the forward and backward reactions. With the reasonable assumption that at room temperature the relative x coordinate of D and I can fluctuate by 1 Å (see Table 1), the ratio of σ values is about 4.

The results of the calculations are summarized in Table 1. The following electron transfer processes are considered:

(*i*) $D^*I \rightarrow D^+I^-$. For this process the largest contribution in Eq. 8 comes at $n_r = 1$ with $E^{\ddagger}(1) \approx 0.1$ kcal/mol.

(*ii*) $D^+I^- \rightarrow DI$. As seen from Fig. 5, this process requires an extremely large activation energy for thermally induced electron transfer to $n_r = 0$ ($E^{\ddagger} \simeq 30$ kcal/mol). Thus, the electron transfer reaction must involve tunneling to excited stretching vibrations of the ground state; the rate is slow because of the tunneling factor $S^{n_r}/n_r!$

(*iii*) $D^+I^-Q \rightarrow D^+IQ^-$. This process involves only r-type stretching modes, and because ΔE_0 is not large, n_r is only 2 and the rate is relatively fast.

(*iv*) $D^+C \rightarrow DC^+$. This reaction, which has been used as a model for electron transfer reactions (4, 5), has an activation energy of 2.8 kcal/mol (as can be estimated from figure 3.10 of ref. 2). The intersection of the corresponding calculated potential surfaces in Fig. 5 gives an activation energy of 10 kcal/mol for $n_r = 0$ and 1.5 kcal/mol for $n_r = 2$. Note that the effective S value for this reaction changes drastically with n_r because the D and D^+ potential surfaces have different curvatures. Thus, the molecular meaning of the S values obtained in previous studies (2, 4, 5) is unclear. These S values, which range from 20 to 48 with corresponding α values of 25–50 kcal/mol, are probably too large for electron transfer in proteins (6).

Discussion

The primary step in bacterial photosynthesis involves an extremely efficient light-induced charge separation. This efficiency might be due, at least in part, to the special form of the dimer potential surfaces. As described schematically in Fig. 5, absorption of light by the DI system creates D^*I, which relaxes to D^+I^- so fast that the competing deactivation of $D^* \rightarrow D$ by radiative or radiationless transitions is prevented. This very fast $D^*I \rightarrow D^+I^-$ process is possible because the intersection of the corresponding potential surfaces occurs at low activation energy. The D^+I^- system is prevented from returning to the DI ground state until the electron is transferred to Q. This is accomplished, in part, by the fact that the D^+I^- and DI potential surfaces intersect along the z direction at very high energy. Finally, D^+ is reduced efficiently by electron transfer from C. The reduction involves surface crossing along the same surface that prevented reduction of D^+ by I^-. This is possible because the intersection between the D and D^+ surfaces depends strongly on ΔE_0; for ΔE_0 of 20 kcal/mol, the surfaces cross at a very steep angle and at high energy (≈30 kcal), whereas for ΔE_0 of 10 kcal/mol, they intersect with a much lower activation energy.[c]

This work analyzed the advantages of the chlorophyll dimer as the primary donor and emphasized the importance of the large changes in the dimer potential surface upon oxidation. In addition, it was pointed out that the change in the electronic matrix element, σ, between the forward and back reactions might play a significant role in the control of the photosynthetic process. However, a similar effect can be obtained with a monomer rather than a dimer as a primary donor.

[b] This type of effect is probably the reason for the large difference in rate between the forward and back light-induced electron transfer between parallel monomers (13).

[c] ΔE_0 for reduction of D^+ by C is probably less than 10 kcal/mol, and the activation energy for $n = 0$ is probably lower than the present estimate.

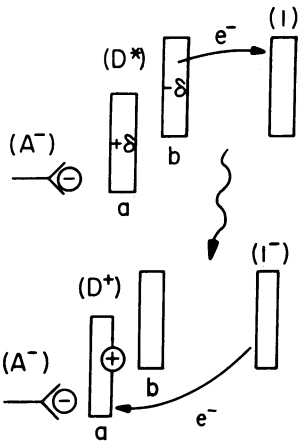

FIG. 6. Possible advantages of interaction between the dimer and an ionized group of the protein (A^-). The polarization of the dimer by A^- increases the charge transfer character of D* and, more importantly, increases the a^+b character of D*, thus slowing the back reaction (see text). In addition, the interaction between A^- and D^+ may pull D^+ further from I^-.

Although I did not consider explicitly the role of the protein, some of its effect is taken into account indirectly by using the experimentally determined ΔE_0, which is affected by the protein (6). Probably the protein is involved in the photosynthetic process in a direct way, as in other biological processes for conversion of light energy to electrostatic energy (14). In this respect it is intriguing to notice that the red shift in the absorption spectrum of the special dimer in bacteria is larger by ≈30 nm than the shift that could be attributed to overlap between the monomers (11). This additional shift is probably due to an ionized acid of the protein, as is the case in other systems (14). Such an ionized acid, A^-, could function in two ways (see Fig. 6). (*i*) The interaction with A^- can polarize the dimer electrons. This will increase the a^+b^- charge transfer character of D* (see ref. 11) and slightly increase σ for the forward reaction. More importantly, the polarization of D^+ will give it more a^+b character,[d] and this will reduce the rate of the back reaction making it correspond to electron transfer from I to the more distant monomer, a (σ for the forward and back reactions will be given approximately by $\langle\phi_b^*|H|\phi_I^*\rangle$ and $\langle\phi_a|H|\phi_I^*\rangle$, where a and b are the monomeric units of D, and ϕ and ϕ^* and the π and π^* molecular orbitals). (*ii*) Another possibility is that the interaction between A^- and D^+ pulls D^+ away from I^-, thus reducing σ for the back reaction.

The present work has demonstrated that the potential surfaces of the dimer system may explain the efficiency of the photosynthetic reaction. However, it was not demonstrated that *only* a dimer can provide such an efficient system. That is, the calculated change in σ between the forward and back reactions can be provided by a monomer. Potential surfaces similar to those presented in Fig. 5 can be obtained with a reaction center of the type A^-DI discussed above, but with a monomer instead of a dimer; the origin shift in the distance between the ionized acid and the monomer replaces the role of z coordinate. It is intriguing to note, however, that the advantage of polarization of D^+ by A^- (see above) is unique to a dimer system.[e] Furthermore, another advantage of the dimer might be its large size; the larger the radius of a charged system in a protein, the smaller the "solvation" by the protein groups (15) and the smaller the expected relaxation of the protein dipoles to stabilize this charge (14). This is advantageous both in minimizing the S values of the protein modes (6) and in minimizing the loss of light energy during the charge separation process (14).

I am grateful to G. Feher and W. W. Parson for introducing me to the exciting field of photosynthesis. This work was supported by Grant GM 24492 from the National Institutes of Health and by the Alfred P. Sloan Foundation.

[d] This is somewhat inconsistent with experimental indication of equal spin distribution on a and b in D^+ (12). However, it is possible that the experimentally determined spin distribution of D^+ corresponds to a "relaxed" protein structure that is different from the structure immediately after excitation.

[e] A primary acceptor composed of two dimers and polarized by an ionized group A^- (i.e., A^-DD) might lead to more efficient light-induced charge separation than an A^-D system.

1. Katz, J. J., Norris, J. R., Shipman, L. L., Thurnauer, M. C. & Wasielewski, M. R. (1978) *Annu. Rev. Biophys. Bioeng.* **7**, 393–434.
2. Blankenship, R. E. & Parson, W. W. (1979) in *Photosynthesis in Relation to Model Systems*, ed. Barber, J. (Elsevier North-Holland, Amsterdam), pp. 71–114.
3. Marcus, R. A. (1964) *Annu. Rev. Phys. Chem.* **15**, 155–196.
4. Hopfield, J. J. (1974) *Proc. Natl. Acad. Sci. USA* **71**, 3640–3644.
5. Jortner, J. (1976) *J. Chem. Phys.* **64**, 4860–4867.
6. Warshel, A. & Weiss, P. M. (1978) in *Frontiers of Biological Energetics*, eds. Dutton, P. L., Leigh, J. S. & Scarpa, A. (Academic, New York), Vol. 1, pp. 30–36.
7. Warshel, A. & Karplus, M. (1972) *Chem. Phys. Lett.* **17**, 7–14.
8. Warshel, A. & Karplus, M. (1975) *Chem. Phys. Lett.* **32**, 11–17.
9. Warshel, A. & Dauber, P. (1977) *J. Chem. Phys.* **66**, 5477–5487.
10. Warshel, A. (1977) in *Modern Theoretical Chemistry*, ed. Segal, G. (Plenum, New York), Vol. 7, pp. 133–171.
11. Warshel, A. (1979) *J. Am. Chem. Soc.* **101**, 744–746.
12. Feher, G., Hoff, A. J., Isaacson, R. A. & Ackerson, L. C. (1975) *Ann. N.Y. Acad. Sci.* **244**, 239–259.
13. Netzel, T. L., Kroger, P., Chang, C. K., Fujita, I. & Fajer, J. (1979) *Chem. Phys. Lett.* **67**, 223–228.
14. Warshel, A. (1979) *Photochem. Photobiol.* **30**, 285–290.
15. Warshel, A. (1978) *Proc. Natl. Acad. Sci. USA* **75**, 5250–5254.